Head-to-Head Comparison of ^{68}Ga-FAPI-46 and ^{18}F-FDG PET/CT for Evaluation of Head and Neck Squamous Cell Carcinoma: A Single-Center Exploratory Study

Chetsadaporn Promteangtrong, Dheeratama Siripongsatian, Attapon Jantarato, Anchisa Kunawudhi, Peerapon Kiatkittikul, Sukanya Yaset, Natphimol Boonkawin, and Chanisa Chotipanich

National Cyclotron and PET Centre, Chulabhorn Hospital, Chulabhorn Royal Academy, Bangkok, Thailand

^{68}Ga-conjugated fibroblast activation protein inhibitor (^{68}Ga-FAPI) has become an attractive agent for PET. This study aimed to compare ^{68}Ga-FAPI-46 PET/CT with ^{18}F-FDG PET/CT for detecting primary cancer and metastatic lesions in patients with head and neck squamous cell carcinoma (HNSCC). **Methods:** Twelve patients and 28 patients with HNSCC underwent ^{68}Ga-FAPI-46 and ^{18}F-FDG PET/CT for initial staging and recurrence detection, respectively. The concordance and diagnostic accuracy of both tracers were analyzed. Semiquantitative parameters, including SUV$_{max}$, SUV$_{mean}$, and tumor-to-background ratio, were compared. Fibroblast activation protein (FAP) expression tumor volume and total lesion FAP expression of ^{68}Ga-FAPI-46 were compared with metabolic tumor volume and total lesion glycolysis of ^{18}F-FDG, respectively. Differences between semiquantitative parameters were analyzed using paired t testing. **Results:** ^{68}Ga-FAPI-46 PET/CT was 83.3% and 96.4% concordant with ^{18}F-FDG PET/CT for initial staging and recurrence detection, respectively. Eighteen lesions had histopathologic validation, and both tracers displayed 100% sensitivity, 50% specificity, and 94.4% accuracy for lesion-based analysis. FAP expression tumor volume was greater than metabolic tumor volume ($P < 0.05$), but no significant differences were observed for the other parameters. **Conclusion:** ^{68}Ga-FAPI-46 PET/CT showed good concordance with, and comparable diagnostic performance to, ^{18}F-FDG PET/CT for initial staging and recurrence detection in HNSCC patients.

Key Words: FAPI; FDG; PET/CT

Head and neck squamous cell carcinoma (HNSCC) is the sixth most common carcinoma worldwide, with 890,000 new cases and 450,000 deaths reported in 2018 (*1*). The treatment of HNSCC depends on the anatomic site, tumor stage, and functional outcome. Early-stage cancers are treated with a single modality, such as surgery or radiotherapy alone, whereas locally advanced cancers require multimodal treatment, which is often a combination of surgery, radiotherapy, and chemotherapy. Therefore, accurate tumor staging is crucial for planning treatment strategies. ^{18}F-FDG PET/CT is a widely accepted tool for imaging various cancers. However, ^{18}F-FDG PET/CT has some limitations when used for HNSCC. High glucose uptake is observed in several normal tissues, such as salivary glands, lymphoid tissues, and lymph nodes. Furthermore, false-positive uptake may occur in areas of peritumoral inflammation or after surgery and radiotherapy (*2*).

The tumor microenvironment in HNSCC is a mix of tumor and stromal cells, including endothelial cells, immune cells, and cancer-associated fibroblasts. Cancer-associated fibroblasts secrete a broad range of growth factors, cytokines, and chemokines that promote tumor growth, angiogenesis, and recruitment of immunosuppressive immune cells and thus have a role in HNSCC invasion and progression (*3*). Fibroblast activation protein (FAP) is overexpressed by cancer-associated fibroblasts in several types of cancer, including HNSCC, with relatively low expression in normal tissue. ^{68}Ga-conjugated FAP inhibitor (FAPI), has been developed for targeting FAP and tumor stromal visualization (*4*). In previous studies, ^{68}Ga-FAPI-04 PET/CT showed a higher sensitivity than ^{18}F-FDG PET/CT in various types of cancers (*5*), and FAPI PET precisely delineated HNSCC for radiotherapy planning (*6*). The aim of this study was to conduct a head-to-head comparison of ^{68}Ga-FAPI-46 PET/CT and standard ^{18}F-FDG PET/CT imaging for detecting primary cancer and metastatic lesions in patients with HNSCC.

MATERIALS AND METHODS

Study Design

This was a single-center exploratory comparative-imaging study. The study was approved by the Human Research Ethics Committee of
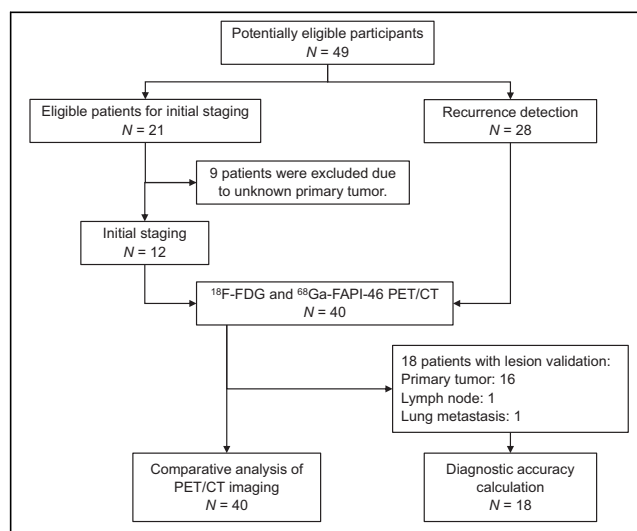
FIGURE 1. Flowchart of study design.

TABLE 1
Characteristics of Study Patients

Patient no.	Age (y)	Sex	Primary tumor	Indication
1	48	M	Tongue	Recurrence detection
2	65	F	Lip	Recurrence detection
3	65	M	Pyriform fossa	Recurrence detection
4	57	M	Tongue	Recurrence detection
5	65	M	Base of tongue	Initial staging
6	57	F	Nasopharynx	Recurrence detection
7	49	F	External ear canal	Recurrence detection
8	35	F	Nasal cavity	Recurrence detection
9	54	F	Nasopharynx	Recurrence detection
10	62	M	Nasopharynx	Recurrence detection
11	69	F	Oropharynx	Initial staging
12	62	F	Tongue	Initial staging
13	58	M	Pyriform fossa	Initial staging
14	79	M	Tongue	Recurrence detection
15	67	M	Pyriform fossa	Recurrence detection
16	77	M	Retromolar trigone	Recurrence detection
17	45	F	Oral mucosa	Initial staging
18	51	M	Nasopharynx	Initial staging
19	59	M	Nasopharynx	Initial staging
20	55	M	Base of tongue	Recurrence detection
21	50	M	Tongue	Initial staging
22	32	F	Nasopharynx	Recurrence detection
23	60	M	Base of tongue	Recurrence detection
24	60	M	Glottis	Recurrence detection
25	61	M	Pyriform fossa	Recurrence detection
26	69	M	Nasopharynx	Recurrence detection
27	63	M	Floor of mouth	Recurrence detection
28	62	M	Pyriform fossa	Initial staging
29	74	M	Nasopharynx	Recurrence detection
30	86	M	Nasopharynx	Recurrence detection
31	55	M	Nasopharynx	Initial staging
32	49	F	Nasopharynx	Recurrence detection
33	53	M	Nasopharynx	Recurrence detection
34	47	M	Nasopharynx	Recurrence detection
35	23	M	Nasopharynx	Recurrence detection
36	42	F	Tongue	Recurrence detection
37	46	M	Nasopharynx	Recurrence detection
38	32	F	Nasopharynx	Recurrence detection
39	51	M	Nasopharynx	Initial staging
40	72	F	Tongue	Initial staging

Study Population

Potentially eligible HNSCC patients were recruited for enrollment in this study from August 2020 through May 2021. The inclusion criteria were pathologically confirmed HNSCC, an age of more than 18 y, and scheduled PET/CT for initial staging or suspected recurrence. Exclusion criteria included a fasting blood sugar of more than 150 mg/dL,
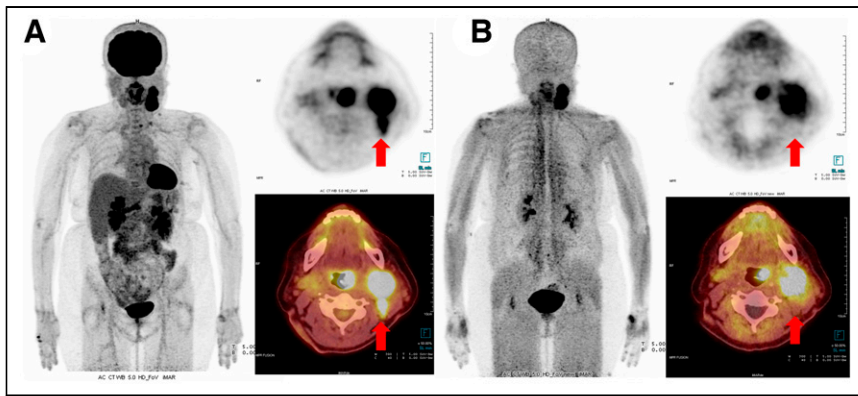
FIGURE 2. ^{18}F-FDG PET/CT (A) and ^{68}Ga-FAPI-46 PET/CT (B) images of 69-y-old woman with left oropharyngeal cancer, stage IVA, who underwent PET/CT for initial staging. ^{18}F-FDG PET/CT detected involved lymph nodes on left side at levels IIA and IIB, whereas ^{68}Ga-FAPI-46 PET/CT did not detect level IIB node (arrows). Left IIB node was confirmed as nodal metastasis by anatomic abnormality criteria.

64-slice Biograph Vision PET/CT scanner (Siemens Healthcare GmbH) in 3-dimensional mode with continuous bed motion, at a speed of 1.6–1.8 mm/s. The matrix was 440 × 440, and the reconstruction methods were True X (Siemens) and time of flight. The CT parameters were a tube voltage of 120 kV, a current of 25 mAs, and a slice thickness of 3.0 mm. ^{68}Ga-FAPI-46 PET/CT was performed for comparative purposes without impacting the final patient management.

PET/CT Imaging Analysis

^{18}F-FDG PET/CT scans were interpreted separately from ^{68}Ga-FAPI-46 PET/CT scans within 2 wk of each other by board-certified nuclear medicine physicians working in consensus. One team interpreted the ^{18}F-FDG PET/CT scans, and a second team interpreted the ^{68}Ga-FAPI-46 PET/CT scans; one of the interpreters was on both teams (5 interpreters total). The interpreters were unaware of the clinical data at the time of review. PET, CT, and PET/CT images were viewed using a Syngo.via workstation (Siemens Healthcare GmbH).

An area of focal uptake visually higher than that of the surrounding background was considered positive. The lesion was categorized as a primary tumor, nodal metastasis, or distant metastasis. Nodal metastasis was classified according to location: neck, supraclavicular, mediastinal, axillary, or intraabdominal. Involvement of the brain, visceral organs in the chest and abdomen, bone, and soft tissues was classified as individual sites. Synchronous and second primary tumors were also analyzed. For initial staging, the clinical TNM stage of HNSCC was based on the eighth edition of the American Joint Committee on Cancer staging system (9).

The 3 designated physicians of each team drew 3-dimensional voxels of interest around the lesions and performed semiquantitative analysis, making adjustments to avoid false-positive results in regions of normal physiologic uptake. The tumor region was delineated automatically using an SUV that was 40% of the SUV_{max}. The SUV_{max}, SUV_{mean}, and tumor-to-background ratio (T/B) of the primary tumor and distant

pregnancy or breast feeding, and unwillingness to participate. The flowchart of the study design is presented in Figure 1.

Preparation of ^{68}Ga-FAPI-46

^{68}Ga-FAPI-46 was synthesized using an iTG [68]Ge/^{68}Ga generator and automated module (iQS-TS; ITM Medical Isotopes) and a good-manufacturing-practice–compliant process, as previously described (7,8) with some modifications.

PET/CT Imaging

^{18}F-FDG and ^{68}Ga-FAPI-46 PET/CT were performed on separate days within a 2-wk period. The patients fasted for 6 h before undergoing ^{18}F-FDG PET/CT, whereas no specific preparation was required for ^{68}Ga-FAPI-46 PET/CT. Before the ^{18}F-FDG PET/CT scan, the plasma glucose level was determined to ensure it was no more than 150 mg/dL. The tracer dose was calculated according to the patient's weight in kilograms (2.59 MBq/kg for ^{18}F-FDG; 2.0 MBq/kg for ^{68}Ga-FAPI-46). Sixty minutes after intravenous administration, scanning was performed from the vertex to the proximal thigh using a

TABLE 2
Comparative ^{18}F-FDG and ^{68}Ga-FAPI-46 PET/CT Results for Initial Staging

Patient no.	Primary tumor	TNM		Stage	
		^{18}F-FDG	^{68}Ga-FAPI-46	^{18}F-FDG	^{68}Ga-FAPI-46
5	Base of tongue	T2N2cM0	T2N2cM0	IVA	IVA
11	Oropharynx	T1N2bM0	T1N2bM0	IVA	IVA
12	Tongue	T3N2cM0	T3N2cM0	IVA	IVA
13	Pyriform fossa	T1N3bM0	T1N3bM0	IVB	IVB
17	Oral mucosa	T3N1M0	T3N1M0	III	III
18	Nasopharynx	T3N2M0	T3N2M0	III	III
19	Nasopharynx	T3N1M0	T3N1M0	III	III
21	Tongue	T3N0M0	T3N0M0	III	III
28	Pyriform fossa	T3N2bM0	T3N2bM1	IVA	IVC
31	Nasopharynx	T2N2M1	T2N1M1	IVB	IVB
39	Nasopharynx	T2N0M0	T2N0M0	II	II
40	Tongue	T2N0M0	T2N0M0	II	II
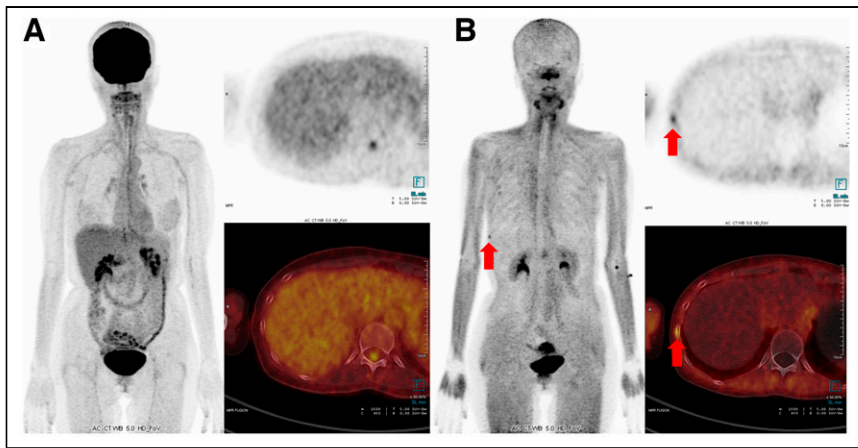
FIGURE 3. ^{18}F-FDG PET/CT (A) and ^{68}Ga-FAPI-46 PET/CT (B) images of 49-y-old woman with nasopharyngeal cancer after concurrent chemoradiation who underwent PET/CT for recurrence detection. ^{68}Ga-FAPI-46 PET/CT showed focal uptake, without corresponding ^{18}F-FDG uptake, in small sclerotic lesion at ninth right lateral rib, which was suspected of being bone metastasis (arrows).

metastases were recorded. T/B was determined by dividing SUV_{max} by the SUV_{mean} of contralateral normal tissue. Metabolic tumor volume (MTV) and total lesion glycolysis assessed by ^{18}F-FDG were compared with the equivalent values assessed by ^{68}Ga-FAPI-46 (FAP expression tumor volume [FTV] and total lesion FAP expression, respectively). The T/B was determined by dividing tumor SUV_{max} by the SUV_{mean} of contralateral normal tissue. MTV and FTV were calculated by multiplying the number of voxels in the tumor region by voxel size. Total lesion glycolysis and total lesion FAP expression were calculated by multiplying MTV or FTV, respectively, by the corresponding SUV_{mean} for each tumor volume. If multiple positive lesions occurred at a single metastatic site, the lesion with the highest activity was analyzed. For nodal metastasis, the SUV_{max} was calculated for each site.

TABLE 3
Comparative ^{18}F-FDG and ^{68}Ga-FAPI-46 PET/CT Results for Recurrence Detection

Patient no.	Primary tumor	Recurrence site	^{18}F-FDG avidity	^{68}Ga-FAPI-46 avidity	PET/CT result
1	Tongue	None	Y	Y	FP
2	Lip	Primary, LN	Y	Y	TP
3	Pyriform fossa	Primary, LN	Y	Y	TP
4	Tongue	Primary, LN	Y	Y	TP
6	Nasopharynx	None	N	N	TN
7	External ear canal	Primary, LN	Y	Y	TP
8	Nasal cavity	None	N	N	TN
9	Nasopharynx	Primary	Y	Y	TP
10	Nasopharynx	Lung	Y	Y	TP
14	Tongue	None	Y	Y	FP
15	Pyriform fossa	Primary	Y	Y	TP
16	Retromolar trigone	Primary, LN	Y	Y	TP
20	Base of tongue	Primary, LN, lung, thyroid	Y	Y	TP
22	Nasopharynx	LN, bone	Y	Y	TP
23	Base of tongue	None	N	N	TN
24	Glottis	Primary, LN	Y	Y	TP
25	Pyriform fossa	LN, liver, adrenal gland	Y	Y	TP
26	Nasopharynx	Primary, LN, lung	Y	Y	TP
27	Floor of mouth	Primary, LN, bone, muscle	Y	Y	TP
29	Nasopharynx	None	N	N	TN
30	Nasopharynx	LN, lung	Y	Y	TP
32	Nasopharynx	Bone	N	Y	FN for ^{18}F-FDG; TP for ^{68}Ga-FAPI
33	Nasopharynx	None	N	N	TN
34	Nasopharynx	LN, nasal turbinate	Y	Y	TP
35	Nasopharynx	None	N	N	TN
36	Tongue	None	N	N	TN
37	Nasopharynx	None	N	N	TN
38	Nasopharynx	LN, lung, pleura	Y	Y	TP

FP = false positive; LN = lymph node; TP = true positive; TN = true negative; FN = false negative.

TABLE 4
Comparative Diagnostic Accuracy of ^{18}F-FDG and ^{68}Ga-FAPI-46 PET/CT

Diagnostic accuracy (%)	^{18}F-FDG	^{68}Ga-FAPI-46
Sensitivity	100	100
Specificity	50	50
Positive predictive value	94.1	94.1
Negative predictive value	100	100
Accuracy	94.4	94.4

Reference Standard

Histopathology served as the gold standard for analysis of diagnostic accuracy. The reference standard for nonbiopsied lesions was the anatomic abnormality observed on CT or MRI. An anatomic criterion for nodal metastasis was either a cluster of at least 3 size-independent nodes at 1 site or fewer than 3 lymph nodes, at least 1 of which measured at least 1 cm along the short axis or had a spheric form or central necrosis. The anatomic criteria for lung metastasis included solid pulmonary nodules, a reticulonodular pattern, cavitating nodules, or lymphangitis carcinomatosis. The anatomic criteria for bone metastasis were lytic or sclerotic lesions with cortical breakthrough, a periosteal reaction, an expansile appearance, pathologic fracture on CT, or an abnormal marrow signal intensity on MRI. The anatomic criterion for distant metastasis was a nodule or mass lesion at another site. Lesions showing focally increased uptake above the background level and with corresponding anatomic criteria were defined as true-positives. Patients with negative PET/CT findings were followed up clinically for at least 3 mo to confirm a true-negative result.

Statistical Analysis

The primary outcome was concordance of ^{8}F-FDG and ^{68}Ga-FAPI-46 PET/CT results for initial staging and recurrence detection. The secondary outcome was the diagnostic accuracy of both tracers. Comparison of semiquantitative parameters was the tertiary outcome.

The visually interpreted PET/CT images were compared with the reference standards. Concordance rates between the 2 tracers for initial staging and recurrence detection were calculated. The diagnostic accuracy of both tracers defined by sensitivity, specificity, positive predictive value, negative predictive value, and accuracy was calculated for lesions with histopathologic validation. Differences in semiquantitative parameters

between ^{18}F-FDG and ^{68}Ga-FAPI-46 PET/CT were analyzed using paired t tests. Data are presented as number or as mean $\pm$ SD. A P value of less than 0.05 was considered statistically significant. STATA software, version 11 (StataCorp LLC), was applied for all analyses.

RESULTS

The characteristics of each patient are shown in Table 1.

Twenty-five primary tumors were detected in 25 patients using both tracers. The mean size of the primary tumors was 3.5 ± 1.4 cm, with a minimum and maximum of 1.5 and 7.4 cm, respectively.

^{18}F-FDG and ^{68}Ga-FAPI-46 identified 128 and 94 lymph nodes, respectively. Overall, there were 33 sites (17 neck, 5 supraclavicular, 1 axillary, 7 mediastinal, and 3 intraabdominal) of nodal involvement in 24 patients detected by both tracers. ^{18}F-FDG PET/CT detected more lymph nodes than did ^{68}Ga-FAPI-46 PET/CT; however, the numbers of sites involved did not differ between the 2 tracers. The sizes of detected nodes ranged from 0.4 to 4.2 cm. Patient with lower nodal detection by ^{68}Ga-FAPI-46 are shown in Figure 2.

Ten of 40 patients presented with distant metastases involving 15 sites (5 pulmonary, 5 bone, 1 pleural, 1 thyroidal, 1 adrenal, 1 hepatic, and 1 muscle). Synchronous tumors were noted in 4 patients (supraglottis in 1 and esophagus in 3). Two patients had a second primary thyroid cancer with histopathologic confirmation. The lesions at each site were detected with both tracers, except for 2 bone lesions in 2 patients that were observed only on ^{68}Ga-FAPI-46 PET/CT. Both bone lesions were confirmed by anatomic criteria for bone metastasis.

Concordance of ^{18}F-FDG and ^{68}Ga-FAPI-46 PET/CT

There was no difference in the assessment of TNM staging between the 2 tracers in 10 of 12 patients, with 83.3% concordance. ^{68}Ga-FAPI-46 PET/CT upstaged 1 patient (patient 28). The upstaged lesion was confirmed by MRI after a marrow change at the right scapula and suspected bone metastasis. In patient 31, ^{68}Ga-FAPI-46 PET/CT detected a lower number of nodal metastases than did ^{18}F-FDG; the multiple nodal metastases were confirmed by anatomic criteria (the size of the 1 discordant node was 1.0 cm in the short axis and 1.2 cm in the long axis). The PET/CT results for initial staging are detailed in Table 2.

A difference in recurrence detection between the 2 tracers was observed in only 1 of 28 patients, with 96.4% concordance. In this patient, ^{68}Ga-FAPI-46 PET/CT showed focal uptake without corresponding ^{18}F-FDG uptake in a sclerotic lesion at the ninth right rib, which was a suspected bone metastasis according to our criteria. Images of the discordant cases are presented in Figure 3. The false-positive results in patient 1 may be explained by postoperative inflammation due to primary-tumor excision about 1 mo before the PET studies. False-positive results with biopsy validation in patient 14 may be explained by postradiation fibrotic changes at 5 mo after radiation. The PET/CT results for recurrence detection are detailed in Table 3.

Diagnostic Accuracy of ^{18}F-FDG and ^{68}Ga-FAPI-46 PET/CT

Eighteen lesions had histopathologic results. Both tracers detected 16 true-positive, 1 true-negative, and 1 false-positive lesions.
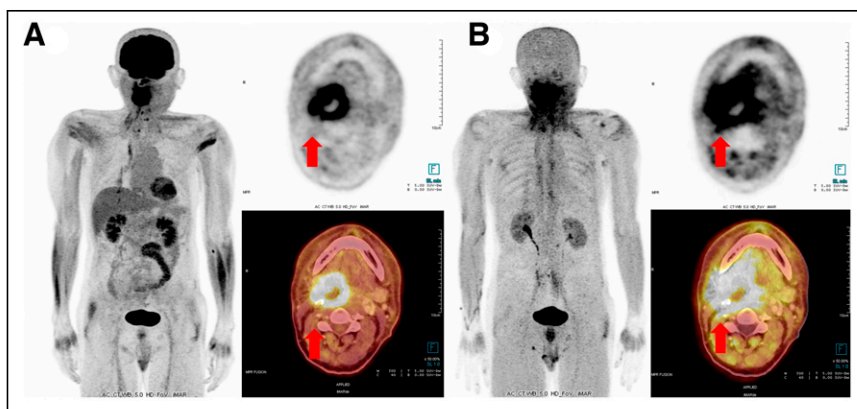
FIGURE 4. ^{18}F-FDG PET/CT (A) and ^{68}Ga-FAPI-46 PET/CT (B) images of 60-y-old man with glottic cancer who underwent PET/CT for recurrence detection. Recurrent tumor avid for ^{18}F-FDG and ^{68}Ga-FAPI-46 was seen at right side of oropharynx (arrows). MTV was 19.37 cm^3. FTV was 33.75 cm^3.

TABLE 5
Comparisons of Semiquantitative Parameters Between ^{18}F-FDG and ^{68}Ga-FAPI-46 PET/CT of Primary Tumor and Distant Metastasis

Parameter	^{18}F-FDG	^{68}Ga-FAPI-46	P
Primary tumor			
SUV$_{max}$	18.59 ± 9.61 (7.15–43.11)	19.28 ± 7.45 (6.40–42.39)	0.65
SUV$_{mean}$	10.82 ± 6.10 (2.54–24.64)	11.10 ± 4.83 (4.17–28.07)	0.78
T/B	10.21 ± 5.89 (1.54–26.37)	11.04 ± 5.03 (2.21–23.51)	0.45
MTV vs. FTV	7.36 ± 5.07 (1.34–21.66)	10.33 ± 9.44 (0.86–35.37)	0.03
TLG vs. TLF	94.91 ± 117.20 (7.14–517.65)	122.58 ± 132.85 (8.88–500.50)	0.06
Distant metastasis			
SUV$_{max}$	13.59 ± 7.64 (3.86–31.69)	16.89 ± 9.96 (3.09–34.22)	0.09
SUV$_{mean}$	7.82 ± 4.45 (2.23–18.42)	9.74 ± 5.67 (1.80–18.18)	0.09
T/B	30.39 ± 55.85 (1.53–254.4)	20.54 ± 13.57 (1.69–52.63)	0.44
MTV vs. FTV	10.52 ± 19.41 (0.18–81.23)	9.02 ± 15.27 (0.25–54.42)	0.33
TLG vs. TLF	109.87 ± 255.52 (1.43–1151.59)	135.92 ± 260.12 (0.78–976.03)	0.36

TLF = total lesion FAP expression (^{68}Ga-FAPI); TLG = total lesion glycolysis (^{18}F-FDG).
Data are mean ± SD followed by range.

No false-negative results were found. The diagnostic accuracy of ^{68}Ga-FAPI-46 and ^{18}F-FDG PET/CT is shown in Table 4.

Comparison of Semiquantitative Parameters

There were no significant differences in semiquantitative parameters, except for the FTV of the primary tumor, which was significantly higher than MTV ($P = 0.03$). An example of a patient with a higher FTV than MTV is shown in Figure 4. The semiquantitative comparisons of primary tumor and distant metastasis are shown in Table 5. The semiquantitative parameters for nodal metastasis are compared in Table 6.

DISCUSSION

To our knowledge, this study was the first head-to-head comparison of diagnostic performance and semiquantitative parameters—such as uptake, image contrast, and tumor volume—between ^{68}Ga-FAPI-46 and ^{18}F-FDG PET/CT in HNSCC patients. ^{68}Ga-FAPI-46 PET/CT had an 83.3% and 96.4% concordance with ^{18}F-FDG PET/CT for initial staging and recurrence detection, respectively. Lesion-based analysis showed comparable diagnostic accuracy. All primary tumors were detected by both tracers. The number of avid nodes detected by ^{68}Ga-FAPI-46 was less than that detected by ^{18}F-FDG. Our findings corresponded with those of Serfling et al. (10), who reported that ^{18}F-FDG PET/CT had a higher detection rate for cervical nodal metastases than did ^{68}Ga-FAPI PET/CT, if the metastatic nodes were smaller than 0.7 cm; smaller nodes resulted in weaker FAP expression and delayed conversion of normal fibroblasts to cancer-associated fibroblasts. However, ^{68}Ga-FAPI-46 may have higher tumor specificity than ^{18}F-FDG, potentially resulting in fewer instances of false-positive uptake in inflamed or otherwise reactive lymph nodes. Differences in detection of avid nodes will require further verification. Our findings were discordant with those of Chen et al. (5), who observed higher sensitivity and lower specificity for nodal metastatic detection by ^{68}Ga-FAPI-04 than by ^{18}F-FDG PET/CT. However, Chen et al. compared ^{68}Ga-FAPI with ^{18}F-FDG PET/CT in various types of cancer, with only 6 HNSCC patients. In our study, ^{68}Ga-FAPI-46 and ^{18}F-FDG PET/CT showed consistency for detection of distant metastases in most cases. However, we

TABLE 6
Semiquantitative Comparisons Between ^{18}F-FDG and ^{68}Ga-FAPI-46 PET/CT for Nodal Metastasis

Site	Median size (cm)	No. of detected nodes		SUV$_{max}$		P
		^{18}F-FDG	^{68}Ga-FAPI-46	^{18}F-FDG	^{68}Ga-FAPI-46	
Neck	1.3	85	56	13.67 ± 7.38	16.91 ± 9.35	0.08
Supraclavicular	0.8	5	4	9.97 ± 3.47	7.16 ± 2.01	
Mediastinal	0.8	30	22	9.21 ± 4.22	8.64 ± 4.54	
Axillary	1.1	3	3	18.64*	10.98*	
Intraabdominal	0.9	5	9	15.83 ± 7.02	31.84 ± 9.00	
All	1.1	128	94	12.55 ± 6.68	15.04 ± 10.25	

*No SD because the SUV$_{max}$ was derived from 1 patient's data.
P value is for SUV$_{max}$. SUV$_{max}$ is mean ± SD.

observed detection differences in 2 bone lesions that showed ^{68}Ga-FAPI-46 avidity but no ^{18}F-FDG uptake. Chen et al. reported a false-positive ^{68}Ga-FAPI–avid bone lesion because of myelofibrosis, which was not observed with ^{18}F-FDG. When histopathologic confirmation is not practical, multimodal imaging is required to obtain morphologic details on metastasis.

Compared with ^{18}F-FDG PET/CT, ^{68}Ga-FAPI-46 PET/CT showed higher contrast images with lower physiologic background in the brain, salivary glands, and Waldeyer ring. However, we found no significant differences between the 2 tracers for SUV$_{max}$, SUV$_{mean}$, T/B, or total lesion glycolysis versus total lesion FAP expression in the primary tumors. No significant differences in these semiquantitative parameters were observed between the tracers for nodal and distant metastases. Although there may be some variation in methods of SUV measurement, our results were consistent with those of Ballal et al. (11), who demonstrated that patients with head and neck cancer had comparably high uptake of ^{68}Ga-DOTA.squaramide-FAPI and ^{18}F-FDG. Our findings did not agree with those of Pang et al. (12), who observed higher uptake of ^{68}Ga-FAPI than of ^{18}F-FDG in primary and metastatic lesions of patients with gastric, duodenal, and colorectal cancers. This difference may be explained by differences in glucose metabolism among various tumor cell types. Pang et al. studied patients with adenocarcinoma or signet-ring cell carcinoma. More than 50% of their subjects were gastric cancer patients who showed low-to-moderate ^{18}F-FDG avidity, whereas our study recruited HNSCC patients, who usually demonstrate high ^{18}F-FDG uptake.

Interestingly, we observed a significantly higher FTV than MTV for the primary HNSCC tumor. Syed et al. (6) used ^{68}Ga-FAPI PET/CT to contour head and neck cancer and found that ^{68}Ga-FAPI–based gross tumor volume was significantly different from CT-based gross tumor volume. When ^{68}Ga-FAPI– and CT-based gross tumor volumes were merged using SUV$_{max}$ thresholds of 3-fold (20%–25% SUV$_{max}$) and 5-fold (40%–50% SUV$_{max}$), the derived tumor volumes were significantly larger than CT-based volumes. We suggest that ^{68}Ga-FAPI-46–derived FTV may be an important semiquantitative parameter for HNSCC, but this possibility will require further standardization and validation.

The sensitivity, specificity, positive predictive value, negative predictive value, and accuracy of both tracers were 100%, 50%, 94.1%, 100%, and 94.4%, respectively. The 8 patients with negative ^{68}Ga-FAPI-46 and ^{18}F-FDG PET/CT findings had no histopathologic confirmation, resulting in low true-negative results and poor specificity in our study.

Our study was limited by the lack of histopathologic confirmation. Use of a fixed 40% threshold of SUV$_{max}$ was dependent on the signal-to-noise ratio, T/B, and tumor size. An adaptive threshold–based method or taking the background into consideration may be more suitable for tumor delineation. A precise definition of FTV is needed for further study. Although there were some limitations in our study, the diagnostic performance of ^{68}Ga-FAPI-46 PET/CT agreed well with that of standard ^{18}F-FDG PET/CT molecular imaging.

CONCLUSION

^{68}Ga-FAPI-46 PET/CT has good concordance with, and comparable diagnostic performance to, ^{18}F-FDG PET/CT for initial staging and recurrence detection in HNSCC patients. Most semiquantitative parameters were comparable between the 2 tracers. However, the ^{68}Ga-FAPI-46–derived FTV was higher than the MTV of ^{18}F-FDG.

Therefore, FTV may be a potential semiquantitative parameter for tumor volume of primary HNSCC, but further standardization and validation are required.

KEY POINTS

QUESTION: Does ^{68}Ga-FAPI-46 PET/CT compare favorably with ^{18}F-FDG PET/CT in HNSCC patients?

PERTINENT FINDINGS: ^{68}Ga-FAPI-46 PET/CT was 83.3% and 96.4% concordant with ^{18}F-FDG PET/CT for initial staging and recurrence detection, respectively. The diagnostic accuracy of ^{68}Ga-FAPI-46 PET/CT was equivalent to that of ^{18}F-FDG PET/CT. ^{68}Ga-FAPI-46–derived FTV was higher than MTV assessed by ^{18}F-FDG, but the other semiquantitative parameters were comparable.

IMPLICATIONS FOR PATIENT CARE: ^{68}Ga-FAPI-46 PET/CT shows comparable diagnostic performance to ^{18}F-FDG PET/CT in detecting primary and metastatic HNSCC.

REFERENCES

1. Ferlay J, Colombet M, Soerjomataram I, et al. Estimating the global cancer incidence and mortality in 2018: GLOBOCAN sources and methods. *Int J Cancer.* 2019;144:1941–1953.
2. Hentschel M, Appold S, Schreiber A, et al. Serial FDG-PET on patients with head and neck cancer: implications for radiation therapy. *Int J Radiat Biol.* 2009;85:796–804.
3. Johnson DE, Burtness B, Leemans CR, Lui VWY, Bauman JE, Grandis JR. Head and neck squamous cell carcinoma. *Nat Rev Dis Primers.* 2020;6:92.
4. Kratochwil C, Flechsig P, Lindner T, et al. ^{68}Ga-FAPI PET/CT: tracer uptake in 28 different kinds of cancer. *J Nucl Med.* 2019;60:801–805.
5. Chen H, Pang Y, Wu J, et al. Comparison of [^{68}Ga]Ga-DOTA-FAPI-04 and [^{18}F] FDG PET/CT for the diagnosis of primary and metastatic lesions in patients with various types of cancer. *Eur J Nucl Med Mol Imaging.* 2020;47:1820–1832.
6. Syed M, Flechsig P, Liermann J, et al. Fibroblast activation protein inhibitor (FAPI) PET for diagnostics and advanced targeted radiotherapy in head and neck cancers. *Eur J Nucl Med Mol Imaging.* 2020;47:2836–2845.
7. Lindner T, Loktev A, Altmann A, et al. Development of quinoline-based theranostic ligands for the targeting of fibroblast activation protein. *J Nucl Med.* 2018;59:1415–1422.
8. Loktev A, Lindner T, Mier W, et al. A tumor-imaging method targeting cancer-associated fibroblasts. *J Nucl Med.* 2018;59:1423–1429.
9. Lydiatt WM, Patel SG, O'Sullivan B, et al. Head and neck cancers: major changes in the American Joint Committee on Cancer eighth edition cancer staging manual. *CA Cancer J Clin.* 2017;67:122–137.
10. Serfling S, Zhi Y, Schirbel A, et al. Improved cancer detection in Waldeyer's tonsillar ring by ^{68}Ga-FAPI PET/CT imaging. *Eur J Nucl Med Mol Imaging.* 2021;48:1178–1187.
11. Ballal S, Yadav MP, Moon ES, et al. Biodistribution, pharmacokinetics, dosimetry of [^{68}Ga]Ga-DOTA.SA.FAPi, and the head-to-head comparison with [^{18}F]F-FDG PET/CT in patients with various cancers. *Eur J Nucl Med Mol Imaging.* 2021;48:1915–1931.
12. Pang Y, Zhao L, Luo Z, et al. Comparison of ^{68}Ga-FAPI and ^{18}F-FDG uptake in gastric, duodenal, and colorectal cancers. *Radiology.* 2021;298:393–402.